minerals

MDPI

Article

The Immobility of Uranium (U) in Metamorphic Fluids Explained by the Predominance of Aqueous U(IV)

Min Zhang, Richen Zhong *, Chang Yu * and Hao Cui

School of Civil and Resource Engineering, University of Science and Technology Beijing, Beijing 100083, China
* Correspondence: zhongrc@ustb.edu.cn (R.Z.); b20200032@xs.ustb.edu.cn (C.Y.)

Abstract: The solubility of uranium (U) in hydrothermal fluid is thought to be controlled by oxidation. In general, uranium is mainly transported as U(VI) in oxidized fluid, but precipitated as U(IV) in reduced fluid. However, many geological observations indicate that metamorphic fluids, which are buffered by metamorphic rocks with oxidized protoliths such as oxidized pelite or altered marine basalt, are not enriched in U. To explore the reason of the low solubility of U in metamorphic fluids, we simulated the hydrous speciation and solubility of U in fluids that are in equilibrium with rocks. The simulations were conducted at pressure–temperature (P-T) conditions of greenschist and amphibolite facies metamorphism. The results show that U is mainly dissolved as U(IV), instead of U(VI), in metamorphic fluids. The solubility of U remains at a low level of ~10^{-12} molal, and is not significantly influenced by metamorphic temperature, pressure, and fluid salinity. This result is consistent with geological observations and, thus, can explain the low-U nature of natural metamorphic fluids. The simulation also shows high solubility of U(VI) (1.3×10^{-7} molal) in oxidized pelite-buffered fluids at low temperature (<250 °C), consistent with the geological fact that U can be mobilized by low-temperature geofluids.

Keywords: uranium speciation; metamorphic fluids; uranium solubility

Citation: Zhang, M.; Zhong, R.; Yu, C.; Cui, H. The Immobility of Uranium (U) in Metamorphic Fluids Explained by the Predominance of Aqueous U(IV). *Minerals* **2023**, *13*, 427. https://doi.org/10.3390/min13030427

Academic Editor: Mauricio Calderón

Received: 8 February 2023
Revised: 9 March 2023
Accepted: 15 March 2023
Published: 17 March 2023

1. Introduction

The hydrothermal mobility of U is mostly governed by its oxidation state. In oxidized fluids, U is exceedingly mobile as a hexavalent uranyle ion (UO_2^{2+}). As far as we know, U might form over 40 types of complexes in fluids, with ligands including hydroxyl, carbonate, sulfate, chloride, phosphate, fluoride, and silicate anions. In reduced fluids, the solubility of U(IV) is extremely low and similar to that of Th, which also has a similar capability during magmatic processes with U [1].

A widely acknowledged model for the formation of unconformity-type uranium deposits involves the interaction of an oxidized basinal brine or meteoric water, which mobilizes the uranium as U(VI), with a reducing, graphite-bearing metapelite that leads to the precipitation of uraninite or other U(IV)-bearing phases such as pitchblende [2–4]. Similarly, the formation of sandstone deposits is mostly controlled by U transport in oxidized surface-derived fluids and deposition when encountering redox barriers, due to a reduction in oxygen fugacity (fO_2) and, therefore, the precipitation of U(IV)-bearing minerals [5].

Previous studies showed that the major element composition of hydrothermal minerals, such as apatite and tourmaline, can record fluid compositions in metasomatic and metamorphic environments [6–10]. Using this approach, it is revealed that metamorphic fluids formed in Barrovian belts are typically depleted in U, with hydrothermal tourmaline and apatite having U contents mostly below the detection limit of LA-ICP-MS (~0.1 ppm) [10–12]. These metamorphic fluids are formed by the devolatilization of hydrous rock piles, mostly pelites or altered basaltic rocks, at the pressure–temperature (P-T) regimes of greenschist to amphibolite facies in orogenic belts. Studies on orogenic gold

deposits, the fluids of which are believed to be products of metamorphic devolatilization, also found that the low-salinity and weakly oxidized gold-forming fluids are not enriched in U [13]. However, the protoliths of metapelites or hydrous metabasalts are either formed in surface environments or altered by sea water, and, therefore, should inherit the oxidizing nature of the exospheres. As a consequence, metamorphic fluids liberated from metapelites or metabasalts should be predominated by the soluble U(VI) and enriched in aqueous U, which are opposite to the geological observations on metamorphic fluids in orogenic belts (e.g., the metamorphic fluids in Barrovian belts).

In this study, to better understand the hydrothermal mobility of U in metamorphic fluids formed in orogenic belts, the hydrous speciation and solubility of U were simulated in metamorphic fluids in equilibrium with metapelites and metabasalts, over a P-T grid of 345 to 650 °C and 0.8 to 5 kbar. The speciation and mobility of aqueous U are significantly influenced by the redox of the fluid, and, thus, three protolith compositions with different redox states are used for simulation, namely average pelite, more oxidized pelite, and altered oceanic basalt. Special focuses were paid on (i) the fluid mobility and the predominant oxidation state of U in metamorphic fluids and (ii) the mechanism controlling the limited mobility of U in fluids released from oxidized metamorphic rocks.

2. Thermodynamic Modeling Methods and Limitation

Thermodynamic equilibrium between metamorphic minerals and an aqueous fluid was calculated using the HCh program, which calculates equilibrium among pure minerals, solid solutions, and a complex aqueous electrolyte solution using the Gibbs energy minimization method. We computed the compositions of the fluid-rock equilibrium in the Al-Ca-Cl-Fe-H-K-Mg-Na-O-Si-U and the Al-Cl-H-K-Mg-Na-O-Si-U systems for basaltic and pelitic protoliths, respectively, over a P-T range of 350–650 °C at an increment of 3 °C and 0.8–5 kbar at 0.04 kbar, respectively. Three bulk rock compositions were selected for thermodynamic modeling (Table 1), namely global average pelite [14], a more oxidized pelite from the Damara Orogen [15], and an altered marine basalt from Pito Deep [16].

Table 1. Bulk compositions used in the thermodynamic modeling (in wt.%, H_2O in access).

	Altered Oceanic Basalt	Average Pelite	Oxidized Pelite
SiO_2	51.98	71.11	59.8
Al_2O_3	14.80	14.38	19.6
MgO	7.65	2.31	1.00
FeO	9.98	7.18	0.60
Fe_2O_3	1.98	0.75	7.30
CaO	10.48	-	-
Na_2O	2.29	-	0.79

In addition, minor amounts of uraninite (UO_2(s)) were added to metamorphic rocks as the source of U in metamorphic fluids. The aqueous species involved in simulations are listed in Tables A1 and A2 in Appendix A for basaltic and pelitic protoliths, respectively. The thermodynamic properties of aqueous species are from the database of Shock et al. [17] and Huang and Sverjensky [18] (Tables A1 and A2 in Appendix A), and those of rock-building minerals or their endmembers are from Holland and Powell [19] (Tables A3 and A4 in Appendix A). The mixing models of solid solutions are listed in Tables A5 and A6 in Appendix A.

At each P-T point, the composition of rock-buffered fluid was calculated at two steps: (i) first, the equilibrium of a solute-free system was calculated with a bulk composition of 100 kg of dry pelite or basic rock (Table 1) and excess pure water. The purpose of the first step is to obtain the water amount required to stabilize the hydrous minerals (e.g., chlorite or muscovite) at the given P-T; (ii) second, minor amounts (1 kg) of free water or H_2O-NaCl solution (with 5 wt.% of dissolved NaCl) were added to the bulk composition of the hydrous pelite or basaltic rocks obtained from the first step. The fluid–rock equilibrium

of these systems is featured by low fluid/rock ratios (1/100), and, thus, the geochemistry of the rock-buffered fluids can be obtained. Two fluids with or without dissolved NaCl were used for the modeling in order to evaluate the influence of fluid chlorine in uranium migration. The NaCl concentration (5 wt.%) was selected because metamorphic fluids in orogenic belts typically have salinities lower than ~7 wt.% NaCl equivalent [20,21].

There are some limitations of the simulation method used in this study. First, restricted by the classical HKF equation of states (EoS; [22]), the modeling was carried out with pressure up to 5 kbar, but the source region of metamorphic fluids extends to crustal depths with higher pressure. For example, the chlorite-out reaction typically takes place at 3.5–7 kbar in orogenic belts, and the pressure required for the reaction increases with higher geothermal gradients [23]. Therefore, the current method limits our ability to accurately examine metamorphic devolatilization in orogenic belts with cooler geothermal conditions. Taking advantage of the knowledge of water densities and dielectric constants at extreme pressure, the DEW model proposed by Sverjensky et al. [24] has extended pressure limitations of the HKF EoS to up to 60 kbar. Along with an empirical method to extrapolate aqueous species' Gibbs free energy to high pressure based on their molar volume at ambient conditions, the DEW model has been successfully applied to predict the geochemical behaviors of geofluids at mantle pressure [25–27]. However, the currently available thermodynamic properties of aqueous U species are regressed based on experiments at low pressure, and it is not clear whether their pressure dependence can be accurately described by the extrapolation given by Sverjensky et al. [24]. Therefore, to guarantee the accuracy of thermodynamic modeling, the traditional HKF EoS is used in this study. Another limitation of the HKF model is that it cannot be applied to low-density fluids [28]. Density contours of 0.5 g/cm^3 are shown in Figures 1 and 2 (green dotted lines) and simulation results are inaccurate at P-T regimes with lower fluid densities, i.e., at the lower pressure and higher temperature side of the contour. Finally, uraninite is assumed to be the only U-bearing mineral in the metamorphic rock in our simulation. However, in metamorphic rocks, large proportions of U exist as trace elements in rock-building minerals such as zircon, monazite, apatite, and xenotime [29–32]. Therefore, in the simulated metamorphic fluids, the U contents are simply controlled by the dissolution of uraninite. This simplification may be established in the cases where uranium is present in metamorphic rocks [33], since U in uraninite is more soluble than those in rock-building minerals, and, thus, controls the U solubility in metamorphic fluids. However, for cases where uraninite is absent, the mobility of U in metamorphic fluids may be overestimated by our simulation results.

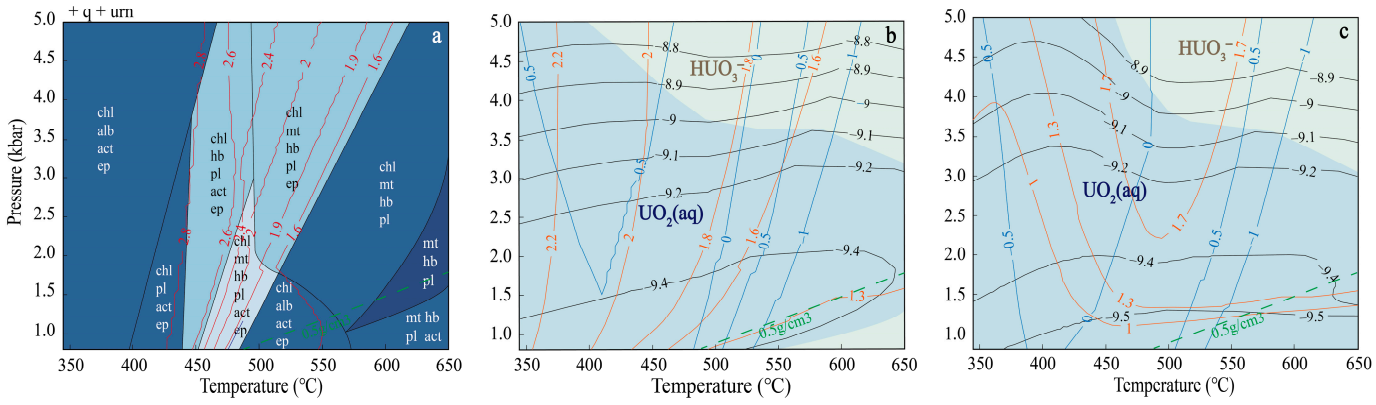

Figure 1. Results of thermodynamic simulation for fluids buffered by altered oceanic basalt. (**a**) P-T pseudosection showing mineral assemblage and content of lithological bound water; (**b**,**c**) solubilities of uranium in pure water and 5 wt.% NaCl-H_2O solution, respectively. The solubility of uranium is shown as logarithm of molality (black line), and the predominance fields of different uranium species are presented by different colors. The orange lines in (**b**,**c**) denote different ΔpH, which is the deviation

of fluid pH from neutral pH (pH_n) ($\Delta pH = pH - pH_n$). The blue lines in (**b**,**c**) denote ΔFMQ, which is the difference in $\log fO_2$ (g) of the fluid relative to the fayalite-magnetite-quartz (FMQ) buffer ($\Delta FMQ = \log fO_2(g)$, fluid $- \log fO_2$, (FMQ)). Bulk rock compositions used for the simulation are given in Table 1. Mineral abbreviations: act = actinolite; alb = albite; chl = chlorite; ep = epidote; hb = hornblende; mt = magnetite; pl = plagioclase; q = quartz; urn = uraninite.

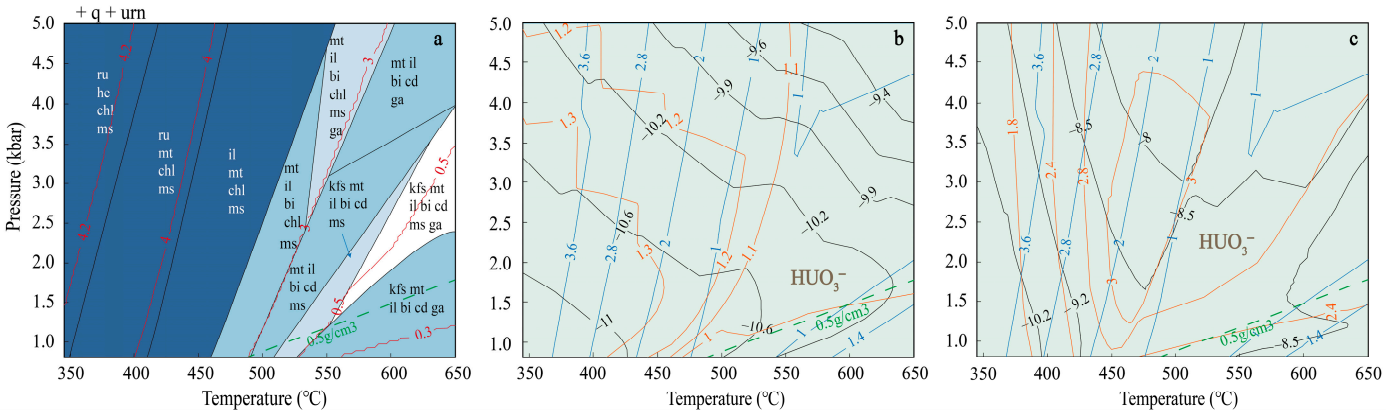

Figure 2. Results of thermodynamic simulation for fluids buffered by typical pelite. (**a**) P-T pseudosection showing mineral assemblage and content of lithological bound water; (**b**,**c**) solubilities of uranium in pure water and 5 wt.% NaCl-H_2O solution, respectively. The solubility of uranium is shown as logarithm of molality (black line), and the predominance fields of different uranium species are presented by different colors.The composition of typical pelite used for the simulation are shown in Table 1. The abbreviations of metamorphic facies: bi = biotite; cd = cordierite; ga = garnet; hem = hematite; il = ilmenite; kfs = K-feldsspar; ms = muscovite; ru = rutile. The other abbreviations are the same as shown for Figure 1. bi = biotite; cd = cordierite; ga = garnet; hem = hematite; il = ilmenite; kfs = K-feldspar; ms = muscovite; ru = rutile.

3. Results

The pseudosection of metabasalt obtained in our simulation (Figure 1a) is consistent with those of previous studies [34,35], and the mineral assemblage in metamorphic phases is consistent with natural observation. For metabasalt, the simulation shows that water is mainly liberated during greenschist facies metamorphism (~450–550 °C at 3 kbar) by decompositions of chlorite and epidote.

As a typical pelite, in accordance with previous studies [21], water is mainly liberated through two dehydration reactions: chlorite decomposition at ~500–550 °C and muscovite decomposition at T > 550 °C at low pressure (Figure 2a). The calculated mineral assemblage and the P-T condition of critical phase transitions (e.g., chlorite-out) are in good agreement with previous studies [36]. Under the P-T condition of interest, the basaltic rock and pelite show typical mineral assemblage, such as greenschist facies, including chlorite, epidote, and muscovite; and amphibolite facies, including hornblende, plagioclase, and quartz.

Since the speciation of aqueous U is influenced by the redox of the fluids, the $\log fO_2$ of the fluids are shown in Figures 1 and 2 and expressed as ΔFMQ (defined as the difference from $\log fO_2$ of the fayalite-magnetite-quartz buffer at the same P-T). The simulation results show that fluids buffered by global average pelite are more oxidized than those by altered oceanic basalt under the greenschist or amphibolite facies conditions. The $\log fO_2$ values of the former are higher than the latter by 0–3 log units (Figures 1 and 2). In both fluids, however, uraninite is dissolved as reduced U(IV) species and has very limited solubility.

Taking the simulation on altered oceanic basalt-buffered fluids for example (Figure 1), the simulation result shows that the solubility of uraninite remains nearly constant (~10^{-9} molal) throughout the P-T conditions of greenschist and amphibolite facies metamorphism, and not significantly influenced by fluid temperature and salinity (Figure 1b,c). In both Cl^--free and Cl^--bearing fluids, aqueous U is predominated by UO_2(aq) under most P-T conditions of interest, and by HUO_3^- at the high-P-T regime (Figure 1b,c). The predominance of

U(IV) species accounts for the insoluble nature U in metamorphic fluids. In Cl^--bearing metamorphic fluids, the predominance of UO_2(aq) or HUO_3^- over chloride complexes indicates that the fluid Cl^- played a minor role in the transport of U, and, therefore, the solubility of uranite in Cl^--bearing fluids is, in general, the same as those in Cl^--free fluids at the same P-T (Figure 1b,c).

In fluids buffered by typical pelite, the solubility of uranium increases slightly with increasing P-T and ranges from 1.3×10^{-3} to 2.5×10^{-2} ppb (Figure 2b), consistent with the low-U nature of metamorphic fluids [10,11]. Uranium in typical pelite mainly exists as HUO_3^- over a P-T range of 350–650 °C and 0.8–5 kbar of the dehydration process (Figure 2b). As a result of the predominance of HUO_3^-, the addition of chlorine to the fluids does not significantly increase the solution of uraninite (Figure 2b,c).

In order to further evaluate the role of protolith redox in U transport in metamorphic fluids, we simulated the speciation and solubility of U in fluids in equilibrium with a more oxidized pelite ("oxidized pelite" in Table 1) over a broader temperature range at constant pressure (25–650 °C and 2 kbar; Figure 3a). Consistent with the simulation results using global average pelite and altered marine basalts, fluids liberated at the P-T conditions of greenschist or amphibolite facies metamorphism are predominated by reduced U(IV) species, HUO_3^-, and are characterized by a very low concentration of aqueous U (~5.2×10^{-3} ppb; Figure 3a). However, at a temperature lower than ~250 °C, fluids buffered by the oxidized pelite are predominated by oxidized U(VI) species, namely HUO_4^-, and, thus, have a much higher solubility of uranite, with aqueous U contents of 35 ppb (Figure 3a).

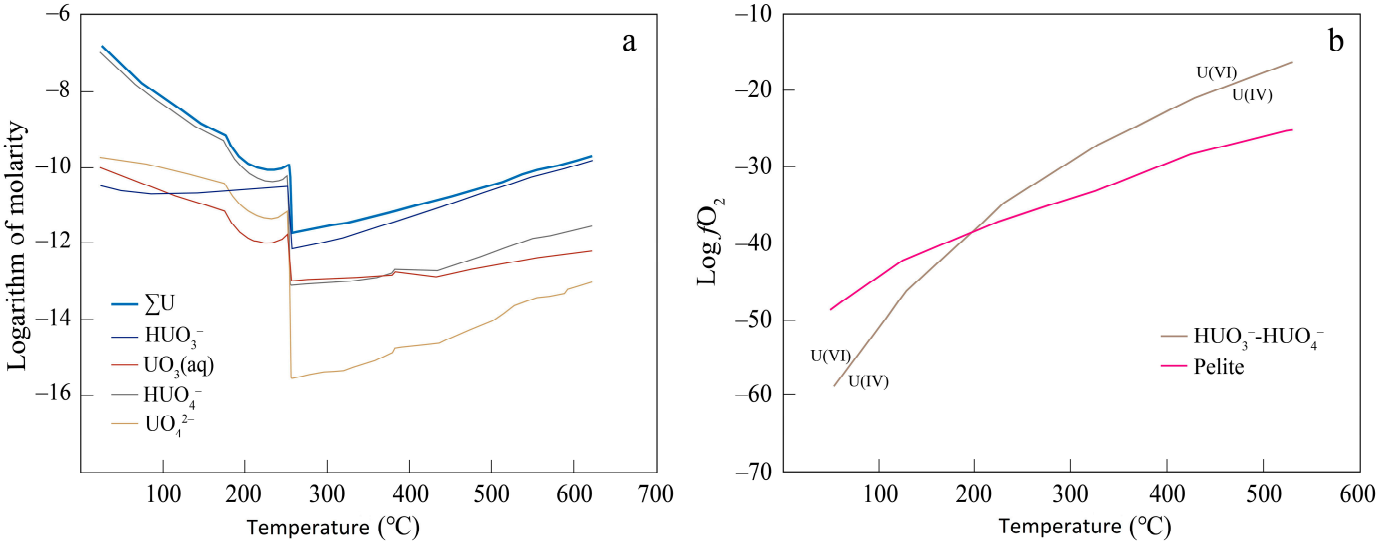

Figure 3. (**a**) The contents of different U-bearing species in fluids released from "oxidized" pelite over a temperature range of 25–650 °C at a constant pressure (2 kbar); (**b**) comparison of calculated logfO_2 of HUO_3^--HUO_4^- and the "oxidized" pelite at different temperatures. The calculated logfO_2 of HUO_3^--HUO_4^- represents the logfO_2 values for the transitions between U(IV) and U(VI).

4. Discussion

It is well known that the oxidizing states of aqueous U have first-order control on its mobility in geofluids, i.e., U-bearing minerals are much more soluble in oxidized fluids that are predominated by U(VI) species than in reduced U(IV)-dominated fluids [5,37]. For example, in U-mineralization systems, the ore-forming fluids are mostly highly oxidized and U(VI)-dominated, with oxygen fugacity (fO_2) above the hematite-magnetite buffer [38,39]. Such an ore-forming model is supported by the geological observation that hematite commonly accompanies U mineralization, whereas magnetite is rarely observed [38]. A possible exception is the case of acidic brines, in which the high mobility of

U can be accounted for by the predominance of U(IV)-chloride complexes even though the fluid is reduced [40].

In our simulation, metamorphic fluids liberated at the P-T regimes of greenschist or amphibolite facies (350–650 °C) are unexceptionally predominated by U(IV) species, namely UO_2(aq) and HUO_3^-, regardless of the lithologies and redox states of the protoliths (Figures 1b,c and 2b,c). As a result, uranite is highly insoluble in greenschist or amphibolite facies metamorphic fluid, with U solubility ranging from 10^{-10} to 10^{-12} molal (~1.3×10^{-3} to 2.5×10^{-2} ppb). Through a comparison between the simulation results of Cl^--free and Cl^--bearing metamorphic fluids, it is revealed that the introduction of Cl^- to the fluid will not significantly enhance the dissolution of uraninite, and U(IV)-chlorides contribute only minor proportions of total aqueous U (~10^{-9}–10^{-11} molal) in typical metamorphic fluids containing 5 wt.% of NaCl (Figures 1c and 2c). This is consistent with the experiment and simulation results by Timofeev et al. [40] that the predominance of U(IV)-chlorides and the consequent high mobility of U in reduced fluids require elevated salinity and acidity of the fluids, but metamorphic fluids sourced from basaltic or basaltic rocks are mostly dilute with salinities of a few weights present of NaCl [41] and weak alkaline with ΔpH ranging from ~1 to ~2.2. These simulation results account for the immobility of U in metamorphic fluids observed from geological samples and the fact that orogenic gold deposits are not enriched in U in ore-forming fluids [13].

In our simulation, the transition from the greenschist face to the amphibolite face causes a drop of the redox state of fluids (e.g., Figure 1), but the metamorphic fluids are still predominated by insoluble U(IV) species even if the protolith is highly oxidized (Figures 1b,c, 2b,c and 3a). However, in fluids buffered by oxidized pelite, U(VI) species become increasingly stable towards lower temperature, and HUO_4^- predominates over U(IV) species at temperatures lower than ~250 °C (Figure 3a,b). The predominant U species changing from U(VI) to U(IV) leads to a significant drop of uranium solubility at ~250 °C (Figure 3a). The dropping temperature of uranium solubility in Figure 3a is not the same as the intersection temperature in Figure 3b, because Figure 3b shows the simulation results of a simple system which only contains HUO_3^- and HUO_4^-, but Figure 3a shows the results of a more complex system which is consistent with geological observation. In consistent with the increasing stability of U(VI) species, the pelite-buffered fluids show an increasingly higher solubility of uranite with reducing temperature. In fluids buffered by oxidized pelite, uranite solubility is as high as ~1.3×10^{-7} molal (i.e., ~35 ppb of U in fluid) at 100 °C, which is about four orders of magnitude higher than those at the temperature of greenschist or amphibolite facies metamorphism. The strong temperature dependence of uranite solubility may account for why the world's vast majority of U deposits are deposited from low-temperature geofluids, such as those of unconformity-, sandstone-, or alkalic-metasomatism-type deposits [37,39,42–44].

The mechanism behind the temperature-controlled U speciation can be illustrated by a comparison between the temperature dependence of fO_2 for rock-buffered fluids and that for the aqueous U(IV)-U(VI) equilibrium (expressed as the fO_2 of fluids with equal activities of HUO_3^- and HUO_4^-). As shown in Figure 3b, fluids buffered by oxidized pelite have fO_2 higher values than the HUO_3^--HUO_4^- equilibrium at temperatures lower than ~180 °C, which implies that the soluble U(VI) species will predominate over the insoluble U(IV) in pelite-buffered fluid at low temperature. On the contrary, at higher temperature, the fO_2 of the pelite-buffered fluids are lower than those of HUO_3^--HUO_4^- and, thus, U(IV) predominates. Conclusively, the different temperature dependences of fO_2 for the rock-dominated system and U-bearing fluids accounts for the predominance of aqueous U(IV) species and, thus, limited mobility of U in fluids liberated during greenschist or amphibolite facies metamorphism.

5. Conclusions

(1) Similar results were obtained in the thermodynamic simulations on geofluids in equilibrium with altered oceanic basalt, global average pelite, and more oxidized pelite,

respectively, in which uranium is dissolved mainly as UO_2(aq) and HUO_3^- in metamorphic fluid, and its solubility is limited to no more than ~2.5×10^{-2} ppb. In addition, the addition of Cl^- cannot significantly improve uranium solubility, and U(IV)-chlorides contribute only minor proportions of total aqueous U.

(2) The comparison between the temperature dependence of fO_2 for rock-buffered fluids and that for the aqueous U(IV)-U(VI) equilibrium indicates that uranium will exist mainly as U(VI), instead of U(IV), in rock-buffered fluids at lower temperatures. This resulted from the different temperature dependence of fO_2 for the rock-dominated system and U-bearing fluids, and leads to a significant enhancement of uranium solubility by four orders of magnitude. This may explain the formation mechanism of low-temperature U deposits in the world.

Author Contributions: Conceptualization, R.Z. and C.Y.; formal analysis, M.Z.; investigation, R.Z., H.C., C.Y. and M.Z.; resources, R.Z.; data curation, M.Z.; writing—original draft preparation, M.Z.; writing—review and editing, R.Z., H.C., C.Y. and M.Z.; funding acquisition, R.Z. and H.C. All authors have read and agreed to the published version of the manuscript.

Funding: This work was supported by the National Natural Science Foundation of China (Nos. 42222303, 41872078, and 42203064), the China Postdoctoral Science Foundation (Grant No. 2022M710350), and the Young Elite Scientists Sponsorship Program by CAST (No. YESS20180143).

Conflicts of Interest: The authors declare no conflict of interest.

Appendix A

Table A1. The aqueous species included in the modeling of altered marine basalt.

Aqueous Species			
H_2O	**$NaHSiO_3$(aq)**	**Al^{3+}**	**$HFeO_2^-$**
H^+	$NaAl_4$(aq)	$AlOH^{2+}$	$FeCl^+$
OH^-	$NaAlO_2$(aq)	$Al(OH)_2^+$	Fe^{3+}
H_2(aq)	Mg^{2+}	$Al(OH)_3$(aq)	$FeOH^+$
O_2(aq)	$MgOH^+$	$Al(OH)_4^-$	$FeOH^{2+}$
$H_3SiO_4^-$	$MgCl^-$	AlO_2^-	$Fe(OH)_3$(aq)
H_4SiO_4(aq)	$MgCl_2$(aq)	AlOOH(aq)	$Fe(OH)_4^-$
SiO_2(aq)	$Mg(HSiO_3)^+$	Fe^{2+}	FeO^+
Cl^-	Ca^{2+}	$FeOH^+$	$HFeO_2$(aq)
Na^+	$CaOH^+$	$Fe(OH)_2$(aq)	$FeCl_2^+$
NaOH(aq)	$CaCl^+$	$Fe(OH)_3^-$	$FeCl_4^-$
NaCl(aq)	$CaCl_2$	FeO(aq)	$FeCl_3$(aq)
U^{3+}	UOH^{2+}	UO_2OH^+	HUO_3^-
UO_2^+	UO^{2+}	$(UO_2)_2(OH)_2^{2+}$	UCl_3^+
UO_2^-	UO^+	UO_2Cl^+	UO_2OH(aq)
U^{4+}	HUO_2(aq)	HUO_2^+	$UO_2Cl_2^-$
UO_2^{2+}	U^{3+}	UO_2(aq)	UO_2Cl_2(aq)
UO_3(aq)	HUO_4^-	UO_4^{2-}	$(UO_2)_2OH^{3+}$

Table A2. The aqueous species included in the modeling of typical and "oxidized" pelite.

Aqueous Species			
H_2O	**$NaHSiO_3$(aq)**	**Al^{3+}**	**$HFeO_2^-$**
H^+	$NaAl_4$(aq)	$AlOH^{2+}$	$FeCl^+$
OH^-	$NaAlO_2$(aq)	$Al(OH)_2^+$	Fe^{3+}
H_2(aq)	Mg^{2+}	$Al(OH)_3$(aq)	$FeOH^+$
O_2(aq)	$MgOH^+$	$Al(OH)_4^-$	$FeOH^{2+}$
$H_3SiO_4^-$	$MgCl^-$	AlO_2^-	$Fe(OH)_3$(aq)
H_4SiO_4(aq)	$MgCl_2$(aq)	AlOOH(aq)	$Fe(OH)_4^-$
SiO_2(aq)	$Mg(HSiO_3)^+$	Fe^{2+}	FeO^+
Cl^-	Ca^{2+}	$FeOH^+$	$HFeO_2$(aq)
Na^+	$CaOH^+$	$Fe(OH)_2$(aq)	$FeCl_2^+$
NaOH(aq)	$CaCl^+$	$Fe(OH)_3^-$	$FeCl_4^-$
NaCl(aq)	$CaCl_2$	FeO(aq)	$FeCl_3$(aq)
U^{3+}	UOH^{2+}	UO_2OH^+	HUO_3^-
UO_2^+	UO^{2+}	$(UO_2)_2(OH)_2^{2+}$	UCl_3^+
UO_2^-	UO^+	UO_2Cl^+	UO_2OH(aq)
U^{4+}	HUO_2(aq)	HUO_2^+	$UO_2Cl_2^-$
UO_2^{2+}	U^{3+}	UO_2(aq)	$(UO_2)_2OH^{3+}$
UO_3(aq)	HUO_4^-	UO_4^{2-}	$KAlO_2$(aq)
UO_2Cl_2(aq)	K^+	KOH(aq)	KCl(aq)
$KAl(OH)_4$(aq)			

Table A3. Pure minerals included in the modeling of altered marine basalt. The thermodynamic properties of the pure minerals are from Holland and Powell [19].

Minerals	Formula
Magnetite (Mt)	Fe_3O_4
Hematite (Hem)	Fe_2O_3
Albite (Alb)	$NaAlSi_3O_8$
Quartz (Qt)	SiO_2
Sillimanite (Sil)	Al_2SiO_5
Kyanite (Ky)	Al_2SiO_5
Andalusite (And)	Al_2SiO_5

Table A4. Pure minerals included in the modeling of typical and "oxidized" pelite. The thermodynamic properties of the pure minerals are from Holland and Powell [19].

Minerals	Formula
Magnetite (Mt)	Fe_3O_4
Hematite (Hem)	Fe_2O_3
K-Feldspar (Kfs)	$KAlSi_3O_8$
Quartz (Qt)	SiO_2
Sillimanite (Sil)	Al_2SiO_5
Kyanite (Ky)	Al_2SiO_5
Sanidine (Sa)	$KAlSi_3O_8$
Andalusite (And)	Al_2SiO_5

Table A5. Solid solutions included in the modeling of altered marine basalt. The thermodynamic properties of end members are from Holland and Powell [19] and Dale et al. [45].

Mineral	End Member	Formula	Activity Model
Chlorite	Daphnite Al-free chlorite Amesite Clinochlore	$Fe_5Al_2Si_3O_{10}$ $Mg_6Si_4O_{10}$ $Mg_4Al_4Si_2O_{10}$ $Mg_5Al_2Si_3O_{10}$	Symmetrical $W_{daphnite}$-$W_{Al\text{-}free\ chlorite}$ = 14.5 $W_{daphnite}$-$W_{amesite}$ = 13.5 $W_{daphnite}$-$W_{clinochlore}$ = 2.5 $W_{Al\text{-}free\ chlorite}$-$W_{amesite}$ = 20 $W_{Al\text{-}free\ chlorite}$-$W_{clinochlore}$ = 18 $W_{amesite}$-$W_{clinochlore}$ = 18
Actinolite	Tremolite Ferroactinolite	$Ca_2Mg_5Si_8O_{22}$ $Ca_2Fe_5Si_8O_{22}$	Ideal
Hornblende	Tremolite Tschermakite Pargasite Glaucophane Ferroactinolite	$Ca_2Mg_5Si_8O_{22}$ $Ca_2Mg_3Al_4Si_6O_{22}$ $NaCa_2Mg_4Al_3Si_6O_{22}$ $Na_2Mg_3Al_2Si_8O_{22}$ $Ca_2Mg_5Si_8O_{22}$	Symmetrical $W_{Tremolite}$-$W_{glaucophane}$ = 65 $W_{tremolite}$-$W_{pargasite}$ = 33 $W_{tremolite}$-$W_{tschermakite}$ = 20 $W_{tremolite}$-$W_{ferroactinolite}$ = 10 $W_{glaucophane}$-$W_{pargasite}$ = 50 $W_{glaucophane}$-$W_{tschermakite}$ = 25 $W_{glaucophane}$-$W_{ferroactinolite}$ = 39.3 $W_{pargasite}$-$W_{tschermakite}$ = −38.5 $W_{pargasite}$-$W_{ferroactinolite}$ = −1.9 $W_{tschermakite}$-$W_{ferroactinolite}$ = 12.5
Plagioclase	Anorthite albite	$CaAl_2Si_2O_8$ $NaAlSi_3O_8$	Symmetrical Wabh-Wan = 3.1
Epidote	Clinozoisite epidote Fe-epidote	$Ca_2Al_3Si_3O_{12}$ $Ca_2FeAl_2Si_3O_{12}Ca_2$ $Fe_2AlSi_3O_{12}$	Symmetrical Wclinozoisite-Wepidote = 0 Wclinozoisite-WFe-epidote = 15.4 Wepidote-WFe-epidote = 3

Table A6. Solid solutions used in the modeling of type and "oxidized" pelite. The thermodynamic properties of end members are from Holland and Powell [19] and White et al. [46].

Mineral	End Member	Formula	Activity Model
Biotite	annite phlogopite eastonite obi tbi fbi	$KFe_3AlSi_3O_{10}$ $KMg_3AlSi_3O_{10}$ $KMg_2Al_3Si_2O_{10}$ $KFeMg_2AlSi_3O_{10}$ $KMg_2TiAlSi_3O_{12}$ $KMg_2Al_2FeSi_2O_{10}$	Symmetrical W_{annite}-$W_{phlogopite}$ = 9 W_{annite}-$W_{eastonite}$ = −1 W_{annite}-W_{obi} = 6 W_{annite}-W_{tbi} = 10 W_{annite}-W_{fbi} = 8 $W_{phlogopite}$-$W_{eastonite}$ = 10 $W_{phlogopite}$-W_{obi} = 3 $W_{eastonite}$-W_{obi} = 10
Chlorite	daphnite Al-free chlorite amesite chlinoclore	$Fe_5Al_2Si_3O_{10}$ $Mg_6Si_4O_{10}$ $Mg_4Al_4Si_2O_{10}$ $Mg_5Al_2Si_3O_{10}$	Symmetrical $W_{daphnite}$-$W_{Al\text{-}free\ chl}$ = 14.5 $W_{daphnite}$-$W_{amesite}$ = 13.5 $W_{daphnite}$-$W_{chlinoclore}$ = 2.5 $W_{Al\text{-}free\ chlorite}$-$W_{amesite}$ = 20 $W_{Al\text{-}free\ chlorite}$-$W_{chlinoclore}$ = 18 $W_{amesite}$-$W_{chlinoclore}$ = 18

Table A6. *Cont.*

Mineral	End Member	Formula	Activity Model
Cordierite	Fe-cordierite hydro cordierite cordierite	$Fe_2Al_4Si_5O_{18}$ $Mg_2Al_4Si_5O_{17}$ $Mg_2Al_4Si_5O_{18}$	Ideal
Garnet	almandine pyrope kho	$Fe_3Al_2Si_3O_{12}$ $Mg_3Al_2Si_3O_{12}$ $Mg_3Fe_2Si_3O_{12}$	Symetrical $W_{amandine}$-W_{pyrope} = 2.5 $W_{amandine}$-W_{kho} = 23
Muscovite	muscovite celadonite Fe-celadonite	$KAl_3Si_3O_{10}$ $KMgAlSi_4O_{10}$ $KFeAlSi_4O_{10}$	Ideal
Staurolite	Fe-staurolite Mg-staurolite	$Fe_4Al_{18}Si_8O_{48}H_2$ $Mg_4Al_{18}Si_8O_{48}H_2$	Symetrical $W_{Fe\text{-}staurolite}$-$W_{Mg\text{-}staurolite}$ = −8
Chloritoid	Fe-ctd Mg-ctd ctdo	$FeAl_2SiO_5$ $MgAl_2SiO_5$ $MgFe_2SiO_5$	$W_{Fe\text{-}ctd}$-$W_{Mg\text{-}ctd}$ = −8

References

1. Langmuir, D. Uranium solution-mineral equilibria at low temperatures with applications to sedimentary ore deposits. *Geochim. Cosmochim. Acta* **1978**, *42*, 547−569. [CrossRef]
2. Bonnetti, C.; Liu, X.; Zhaobin, Y.; Cuney, M.; Michels, R.; Malartre, F.; Mercadier, J.; Cai, J. Coupled uranium mineralisation and bacterial sulphate reduction for the genesis of the Baxingtu sandstone-hosted U deposit, SW Songliao Basin, NE China. *Ore Geol. Rev.* **2017**, *82*, 108–129. [CrossRef]
3. Cui, T.; Yang, J.; Samson, I.M. Tectonic deformation and fluid flow: Implications for the formation of unconformity-related uranium deposits. *Econ. Geol.* **2012**, *107*, 147–163. [CrossRef]
4. Ruzicka, V. Monometallic and polymetallic deposits associated with the sub-Athabasca unconformity in Saskatchewan. *Geol. Surv. Can. Paper* **1989**, *1*, 67−79.
5. Cuney, M.; Mercadier, J.; Bonnetti, C. Classification of sandstone-related uranium deposits. *J. Earth Sci.* **2022**, *33*, 236−256. [CrossRef]
6. Taylor, B.E.; Slack, J.F. Tourmalines from appalachian-caledonian massive sulfide deposits; textural, chemical, and isotopic relationships. *Econ. Geol.* **1984**, *79*, 1703−1726. [CrossRef]
7. Lottermoser, B.; Plimer, I. Chemical variation in tourmalines, Umberatana, South Australia. *Neues Jahrb. Für Mineral. Mon.* **1987**, *7*, 314−326.
8. Gallagher, V.; Kennan, P. Tourmaline on the margin of the Leinster Granite, southeast Ireland: Petrogenetic implications. *Irish J. Earth Sci.* **1992**, *11*, 131−150.
9. Slack, J.F.; Coad, P.R. Multiple hydrothermal and metamorphic events in the Kidd Creek volcanogenic massive sulphide deposit, Timmins, Ontario: Evidence from tourmalines and chlorites. *Can. J. Earth Sci.* **1989**, *26*, 694−715. [CrossRef]
10. Zheng, J.; Shen, P.; Feng, W. Hydrothermal apatite record of ore-forming processes in the Hatu orogenic gold deposit, West Junggar, Northwest China. *Contrib. Miner. Petrol.* **2022**, *177*, 27. [CrossRef]
11. Hazarika, P.; Mishra, B.; Pruseth, K.L. Diverse tourmaline compositions from orogenic gold deposits in the Hutti-Maski greenstone belt, India: Implications for sources of ore-forming fluids. *Econ. Geol.* **2015**, *110*, 337−353. [CrossRef]
12. Sciuba, M.; Beaudoin, G.; Makvandi, S. Chemical composition of tourmaline in orogenic gold deposits. *Miner. Deposita* **2021**, *56*, 537−560. [CrossRef]
13. McGloin, M.V.; Tomkins, A.G.; Webb, G.P.; Spiers, K.; MacRae, C.M.; Paterson, D.; Ryan, C.G. Release of uranium from highly radiogenic zircon through metamictization: The source of orogenic uranium ores. *Geology* **2016**, *44*, 15−18. [CrossRef]
14. White, R.; Powell, R.; Holland, T. Calculation of partial melting equilibria in the system Na_2O–CaO–K_2O–FeO–MgO–Al_2O_3–SiO_2–H_2O (NCKFMASH). *J. Metamorph. Geol.* **2001**, *19*, 139−153. [CrossRef]
15. Haack, U.; Heinrichs, H.; Boness, M.; Schneider, A. Loss of metals from pelites during regional metamorphism. *Contrib. Miner. Petrol.* **1984**, *85*, 116−132. [CrossRef]
16. Barker, A.; Coogan, L.; Gillis, K. Insights into the behaviour of sulphur in mid-ocean ridge axial hydrothermal systems from the composition of the sheeted dyke complex at Pito Deep. *Chem. Geol.* **2010**, *275*, 105−115. [CrossRef]
17. Shock, E.L.; Sassani, D.C.; Betz, H. Uranium in geologic fluids: Estimates of standard partial molal properties, oxidation potentials, and hydrolysis constants at high temperatures and pressures. *Geochim. Cosmochim. Acta* **1997**, *61*, 4245−4266. [CrossRef]
18. Huang, F.; Sverjensky, D.A. Extended deep earth water model for predicting major element mantle metasomatism. *Geochim. Cosmochim. Acta* **2019**, *254*, 192−230. [CrossRef]

19. Holland, T.; Powell, R. An internally consistent thermodynamic data set for phases of petrological interest. *J. Metamorph. Geol.* **1998**, *16*, 309−343. [CrossRef]
20. Goldfarb, R.J.; Baker, T.; Dubé, B.; Groves, D.I.; Hart, C.J.; Gosselin, P. Distribution, character, and genesis of gold deposits in metamorphic terran. *Econ. Geol.* **2005**, 407–475. [CrossRef]
21. Zhong, R.; Brugger, J.; Chen, Y.; Li, W. Contrasting regimes of Cu, Zn and Pb transport in ore-forming hydrothermal fluids. *Chem. Geol.* **2015**, *395*, 154−164. [CrossRef]
22. Tanger, J.C.; Helgeson, H.C. Calculation of the thermodynamic and transport properties of aqueous species at high pressures and temperatures; revised equations of state for the standard partial molal properties of ions and electrolytes. *Am. J. Sci.* **1988**, *288*, 19−98. [CrossRef]
23. Tomkins, A.G. Windows of metamorphic sulfur liberation in the crust: Implications for gold deposit genesis. *Geochim. Cosmochim. Acta* **2010**, *74*, 3246−3259. [CrossRef]
24. Sverjensky, D.A.; Harrison, B.; Azzolini, D. Water in the deep Earth: The dielectric constant and the solubilities of quartz and corundum to 60 kb and 1200 °C. *Geochim. Cosmochim. Acta* **2014**, *129*, 125−145. [CrossRef]
25. Zhong, R.; Li, Y.; Etschmann, B.; Brugger, J.; Yu, C.; Cui, H. HighPGibbs, a practical tool for fluid-rock thermodynamic simulation in deep Earth and its application on calculating nitrogen speciation in subduction zone fluids. *Geochem. Geophys. Geosyst.* **2020**, *21*, e2020GC008973. [CrossRef]
26. Galvez, M.E.; Connolly, J.A.; Manning, C.E. Implications for metal and volatile cycles from the pH of subduction zone fluids. *Nature* **2016**, *539*, 420−424. [CrossRef] [PubMed]
27. Connolly, J.A.; Galvez, M.E. Electrolytic fluid speciation by Gibbs energy minimization and implications for subduction zone mass transfer. *Earth Planet. Sci. Lett.* **2018**, *501*, 90−102. [CrossRef]
28. Shock, E.L.; Helgeson, H.C. Calculation of the thermodynamic and transport properties of aqueous species at high pressures and temperatures: Correlation algorithms for ionic species and equation of state predictions to 5 kb and 1000 °C. *Geochim. Cosmochim. Acta* **1988**, *52*, 2009−2036. [CrossRef]
29. Giles, D.; Nutman, A.P. SHRIMP U–Pb monazite dating of 1600–1580 Ma amphibolite facies metamorphism in the southeastern Mt Isa Block, Australia. *Aust. J. Earth Sci.* **2002**, *49*, 455−465. [CrossRef]
30. Bingen, B.; Demaiffe, D.; Hertogen, J. Redistribution of rare earth elements, thorium, and uranium over accessory minerals in the course of amphibolite to granulite facies metamorphism: The role of apatite and monazite in orthogneisses from southwestern Norway. *Geochim. Cosmochim. Acta* **1996**, *60*, 1341−1354. [CrossRef]
31. O'Sullivan, G.; Chew, D.; Kenny, G.; Henrichs, I.; Mulligan, D. The trace element composition of apatite and its application to detrital provenance studies. *Earth Sci. Rev.* **2020**, *201*, 103044. [CrossRef]
32. Pyle, J.M.; Spear, F.S.; Rudnick, R.L.; Mcdonough, W.F. Monazite–xenotime–garnet equilibrium in metapelites and a new monazite–garnet thermometer. *J. Petrol.* **2001**, *42*, 2083−2107. [CrossRef]
33. Mercadier, J.; Annesley, I.; McKechnie, C.; Bogdan, T.; Creighton, S. Magmatic and metamorphic uraninite mineralization in the western margin of the Trans-Hudson orogen (Saskatchewan, Canada): A uranium source for unconformity-related uranium deposits? *Econ. Geol.* **2013**, *108*, 1037−1065. [CrossRef]
34. Diener, J.; Powell, R.; White, R.; Holland, T. A new thermodynamic model for clino-and orthoamphiboles in the system Na_2O–CaO–FeO–MgO–Al_2O_3–SiO_2–H_2O–O. *J. Metamorph. Geol.* **2007**, *25*, 631−656. [CrossRef]
35. Wei, C.; Duan, Z. Phase relations in metabasic rocks: Constraints from the results of experiments, phase modeling and ACF analysis. *Geol. Soc. Lond. Spec. Pub.* **2019**, *474*, 25−45. [CrossRef]
36. Zhong, R.; Brugger, J.; Tomkins, A.G.; Chen, Y.; Li, W. Fate of gold and base metals during metamorphic devolatilization of a pelite. *Geochim. Cosmochim. Acta* **2015**, *171*, 338−352. [CrossRef]
37. Cuney, M. The extreme diversity of uranium deposits. *Miner. Deposita* **2009**, *44*, 3−9. [CrossRef]
38. Richard, A.; Rozsypal, C.; Mercadier, J.; Banks, D.A.; Cuney, M.; Boiron, M.-C.; Cathelineau, M. Giant uranium deposits formed from exceptionally uranium-rich acidic brines. *Nat. Geosci.* **2012**, *5*, 142−146. [CrossRef]
39. Komninou, A.; Sverjensky, D. Geochemical modeling of the formation of an unconformity-type uranium deposit. *Econ. Geol.* **1996**, *91*, 590−606. [CrossRef]
40. Timofeev, A.; Migdisov, A.A.; Williams-Jones, A.E.; Roback, R.; Nelson, A.T.; Xu, H. Uranium transport in acidic brines under reducing conditions. *Nat. Commun.* **2018**, *9*, 1469. [CrossRef]
41. Evans, K.A.; Tomkins, A.G. Metamorphic fluids in orogenic settings. *Elements* **2020**, *16*, 381−387. [CrossRef]
42. Hoeve, J.; Sibbald, T.I. On the genesis of Rabbit Lake and other unconformity-type uranium deposits in northern Saskatchewan, Canada. *Econ. Geol.* **1978**, *73*, 1450−1473. [CrossRef]
43. Hostetler, P.; Garrels, R. Transportation and precipitation of uranium and vanadium at low temperatures, with special reference to sandstone-type uranium deposits. *Econ. Geol.* **1962**, *57*, 137−167. [CrossRef]
44. Cui, H.; Zhong, R.; Xie, Y.; Wang, X.; Chen, H. Melt–fluid and fluid–fluid immiscibility in a Na_2SO_4–SiO_2–H_2O system and implications for the formation of rare earth deposits. *Acta Geol. Sin-Engl.* **2021**, *95*, 1604−1610.

45. Dale, J.; Powell, R.; White, R.; Elmer, F.; Holland, T. A thermodynamic model for Ca–Na clinoamphiboles in Na_2O–CaO–FeO–MgO–Al_2O_3–SiO_2–H_2O–O for petrological calculations. *J. Metamorph. Geol.* **2005**, *23*, 771−791. [CrossRef]
46. White, R.; Powell, R.; Holland, T.; Worley, B. The effect of TiO_2 and Fe_2O_3 on metapelitic assemblages at greenschist and amphibolite facies conditions: Mineral equilibria calculations in the system K_2O–FeO–MgO–Al_2O_3–SiO_2–H_2O–TiO_2–Fe_2O_3. *J. Metamorph. Geol.* **2000**, *18*, 497−511. [CrossRef]